nature materials

ARTICLES

PUBLISHED ONLINE: 10 MARCH 2013 | DOI: 10.1038/NMAT3570

Stacked topological insulator built from bismuth-based graphene sheet analogues

Bertold Rasche[1], Anna Isaeva[1], Michael Ruck[1,2], Sergey Borisenko[3], Volodymyr Zabolotnyy[3], Bernd Büchner[3,4], Klaus Koepernik[3], Carmine Ortix[3], Manuel Richter[3] and Jeroen van den Brink[3,4]*

Commonly, materials are classified as either electrical conductors or insulators. The theoretical discovery of topological insulators has fundamentally challenged this dichotomy. In a topological insulator, the spin–orbit interaction generates a non-trivial topology of the electronic band structure dictating that its bulk is perfectly insulating, whereas its surface is fully conducting. The first topological insulator candidate material put forward—graphene—is of limited practical use because its weak spin–orbit interactions produce a bandgap of ∼0.01 K. Recent reexaminations of Bi_2Se_3 and Bi_2Te_3, however, have firmly categorized these materials as strong three-dimensional topological insulators. We have synthesized the first bulk material belonging to an entirely different, weak, topological class, built from stacks of two-dimensional topological insulators: $Bi_{14}Rh_3I_9$. Its Bi–Rh sheets are graphene analogues, but with a honeycomb net composed of $RhBi_8$ cubes rather than carbon atoms. The strong bismuth-related spin–orbit interaction renders each graphene-like layer a topological insulator with a 2,400 K bandgap.

As well as being new states of matter and thus of the most fundamental scientific interest[1–5], topological insulators also hold promise for applications in, for instance, spintronics, based on the fact that the topological properties dictate that the metallic surface states of topological insulators are spin-locked: theory predicts that the propagation direction of surface electrons is robustly linked to their spin orientation[3–6]. These surface states also play a most prominent role in proposals to create Majorana fermions in microelectronic devices, the manipulation of which can be the basis for future topological quantum computing[7–9].

In spite of this conceptual richness, a lack of equivalent advances in producing new classes of topological insulator materials has led materials synthesis and chemistry to concentrate largely on further perfecting and varying the materials class of bismuth-based chalcogenides Bi_2Se_3 and Bi_2Te_3, which are confirmed three-dimensional (3D) topological insulators[10–13], and HgTe films grown with utmost care by molecular beam epitaxy that under specific conditions form a 2D topological insulator[14,15]. We have synthesized $Bi_{14}Rh_3I_9$, which we will show to be the first member of an entirely new class of stacked 2D topological insulators, from a stoichiometric melt of its elements. The resulting thin black platelets are air-stable and can be easily cleaved. The synthetic procedure has been optimized taking into account the phase decomposition at the peritectic point of 441°C and the strong dependence of the phase stability on the vapour pressure. For a more detailed synthesis protocol, see Supplementary Information.

The crystal structure was determined by single-crystal X-ray diffraction and exhibits a periodic alternating stacking of 2D bismuth–rhodium networks and insulating spacers (Fig. 1a). The former, further denoted as the intermetallic layer, can be understood as a decorated honeycomb network. It has the same hexagonal *p6/mmm* layer group symmetry as a graphene sheet, thus sharing its 24 symmetry elements. A lattice scaling of ∼3.8 in Fig. 1b makes this structural equivalence prominent. Whereas the nodes of a graphene sheet host carbon atoms, in the intermetallic layer of $Bi_{14}Rh_3I_9$ the nodes of the net are found in the centres of triangular–prismatic voids (Bi–Bi: 317.5–320.6 pm). These appear in the hexagonal arrangement of bismuth cubes (Bi–Bi: 317.5–345.3 pm) that are centred by rhodium atoms (Rh–Bi: 282.0–284.9 pm). This arrangement can also be seen as a kagome-type net with the rhodium atoms of edge-sharing cubes at the nodes of the net. Consequently, the $RhBi_8$ cubes define the hexagonal–prismatic voids that are filled with iodide anions (Bi···I: 376.2–382.1 pm). As a result, an overall composition of $[(RhBi_4)_3I]$ can be assigned to the intermetallic layer. Chemical-bonding analysis reveals strongly localized, covalent Bi–Rh bonds in the cubes and three-centred bismuth interactions in the bases of the triangular–prismatic voids, all together establishing a quasi-2D bimetallic network (see Supplementary Information for details). The spacer layer consists of Bi–I zigzag chains with distorted octahedral coordination of bismuth(III) cations by iodide anions. Bismuth–iodine distances between the intermetallic layer and the spacer (376.4–455.6 pm, mean value 401.9 pm) point at weak interactions of charged layers and render the whole sandwiched structure of $Bi_{14}Rh_3I_9 = [(RhBi_4)_3I]^{2+}[Bi_2I_8]^{2-}$ as salt-like in stacking direction. The alternate stacking of the highly symmetric intermetallic and the low-symmetric spacer layer results in the reduction of the overall crystal symmetry to the triclinic space group $P\bar{1}$.

The fact that the weakly coupled intermetallic layers have the same structural symmetry as graphene sheets suggests similarities in electronic structure between graphene and $Bi_{14}Rh_3I_9$. Indeed, a scalar relativistic band-structure calculation for $Bi_{14}Rh_3I_9$, where the spin–orbit coupling (SOC) is effectively switched off (for details see Supplementary Information), reveals the presence of two Dirac cones in the triclinic Brillouin zone, which are situated at the Fermi level (Fig. 2a). Unfolding the triclinic zone to a hexagonal one, we observe that the two inequivalent Dirac cones appear very

[1]Department of Chemistry and Food Chemistry, TU Dresden, D-01062 Dresden, Germany, [2]Max Planck Institute for Chemical Physics of Solids, D-01187 Dresden, Germany, [3]Leibniz Institute for Solid State and Materials Research, IFW Dresden, D-01069 Dresden, Germany, [4]Department of Physics, TU Dresden, D-01062 Dresden, Germany. *e-mail: j.van.den.brink@ifw-dresden.de.

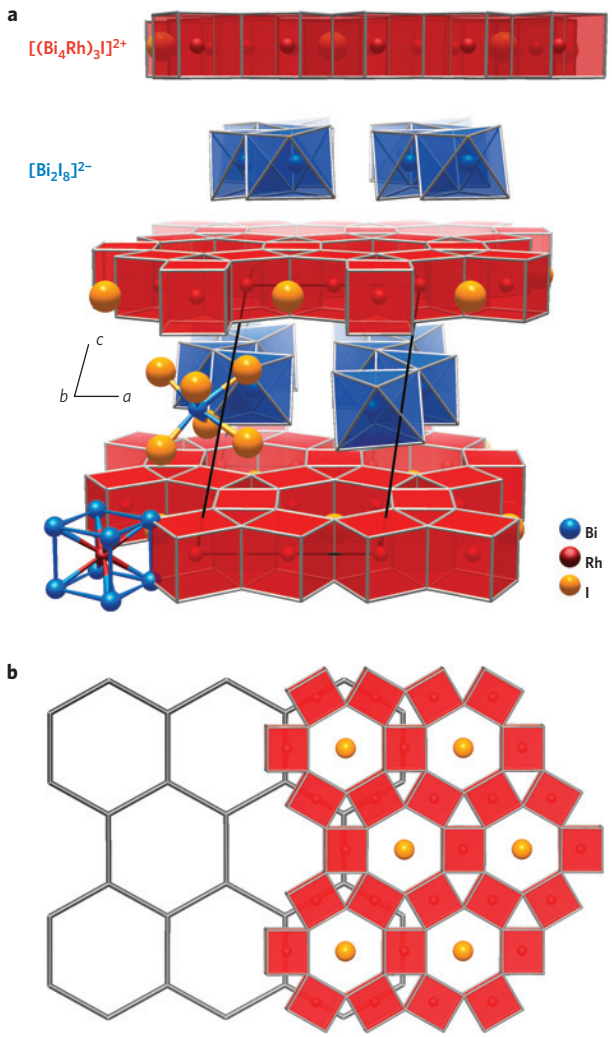

Figure 1 | Structure of $Bi_{14}Rh_3I_9$ and its relation to graphene. a, Triclinic crystal structure of $Bi_{14}Rh_3I_9$. Insulating layers of $[Bi_2I_8]^{2-}$ zigzag chains separate the intermetallic $[(RhBi_4)_3I]^{2+}$ layers that consist of hexagonal nets of edge-sharing $RhBi_8$ cubes. **b**, Honeycomb lattice of graphene scaled by a factor ~3.8 overlaid with the structure of the intermetallic layer.

close to the K and K′ point at the edge of the hexagonal Brillouin zone, precisely where they are in graphene (Fig. 2c). The very weak hopping of electrons between the layers causes the Dirac cones to pick up a minor dispersion perpendicular to the plane, rendering the calculated band structure quasi-2D.

However, for a proper understanding of the electronic band structure one needs to go beyond calculations in scalar relativistic approximation. Whereas the relativistic SOC in, for instance, graphene is very weak—it is expected to open a gap on an energy scale[16] of 0.01 K—bismuth is well known for its strong SOC that can drive and stabilize topologically non-trivial electronic states. As we are thus dealing with graphene-like Dirac cones in the presence of strong SOC, the mechanism proposed in ref. 2 to stabilize a topologically non-trivial quantum spin Hall state will be in action full-force in the intermetallic layers of $Bi_{14}Rh_3I_9$. Indeed, a full relativistic band-structure calculation reveals a gapping out of the Dirac cones, resulting in a calculated bandgap of 210 meV, corresponding to 2,400 K, see Fig. 2b.

To confirm the topological nature of the resulting insulating state we have implemented the direct calculation of the four topological Z_2 invariants[5,17–19] $\nu_0;(\nu_1,\nu_2,\nu_3)$ in the full-potential local-orbital (FLPO) band-structure code[20] (see Supplementary Information for details). This calculation is based on an analysis of the wavefunction parity eigenvalues at the eight time-reversal invariant points of the band structure, as illustrated in Fig. 2f. Owing to the stacking of the quasi-2D intermetallic planes in which SOC has gapped out the Dirac cones, one expects $Bi_{14}Rh_3I_9$ to be a weak topological insulator and indeed we find $\nu_0 = 0$. The other topological invariants are calculated to be $(\nu_1,\nu_2,\nu_3) = (0,0,1)$. The fact that $\nu_0 = 0$ and $\nu_3 = 1$ proves that $Bi_{14}Rh_3I_9$ is a weak topological insulator—the first synthesized material in this topological class—and confirms that the intermetallic planes form sheets of quantum spin Hall states that are stacked along the c axis. It implies that in the Altland–Zirnbauer classification[21] $Bi_{14}Rh_3I_9$ belongs to the symplectic (AII) topology class. On surfaces perpendicular to the normal (001)—and therefore parallel to the intermetallic planes, which are the natural cleaving planes of the material—topological surface states will thus be absent. At any other surface an even number of Dirac cones appears, each having a strongly anisotropic group velocity due to the quasi-2D nature of the bulk band structure. The metallicity of these surface states is stable against disorder, which, as for strong topological insulators in the symplectic class, does not act as a source of localization[22,23].

The band structure obtained from the electronic-structure calculations can be tested experimentally by angle-resolved photoemission spectroscopy (ARPES), which in particular can provide the experimental value of the electronic bandgap, if by slight electron doping the Fermi level of the material is pushed into the conduction band. The ARPES spectra in Fig. 3a,d are consistent with the material being n-doped, which can be due to a slight iodine deficiency related to its vapour pressure or alternative causes for charge redistribution at the surface probed by ARPES.

We compare the ARPES results with the fully relativistic band-structure calculations in the unfolded Brillouin zone selecting the ΓK high-symmetry direction (Fig. 3a,b, for other cuts see Supplementary Information). This is a direction where the Dirac cones are found in scalar relativistic approximation. The agreement between experimental data and full relativistic calculations is remarkable. First, the observed gap, as determined considering the distance between the features of the integrated (over three Brillouin zones) spectral weight, is ~270 meV, which is consistent with the relativistic band structure. Also the number and behaviour of the dispersing features clearly seen in ARPES intensity plots are essentially captured by the bands projected to the hexagonal Brillouin zone. The prominent examples are the inequivalence of Γ and Γ_2 points and structures between K and K_2, both also present in the calculated band structure.

This agreement confirms experimentally the validity of the calculated band structure in the presence of SOC—the bands for which we have calculated the topological invariants to be $\nu_0;(\nu_1,\nu_2,\nu_3) = 0;(0,0,1)$. This topologically non-trivial state is understood in terms of the graphene-like structure of the intermetallic Bi–Rh planes, for which two Dirac cones are present at the Fermi level in a calculation without SOC. Experimentally the SOC is of course unavoidable and switching it on in the calculation gaps out the Dirac cones and generates the weak topological $0;(0,0,1)$ state. As a consequence spin-locked topological surface states will be present at any crystal face that is not parallel to the (001) plane. Such faces, however, do not correspond to natural cuts of the crystal and the associated surface roughness has prevented us so far from observing these spin-polarized surface states by ARPES on, for instance, (100) surfaces. In principle, (spin-polarized) scanning tunnelling microscopy and spectroscopy should be able to directly probe these states at step edges of the natural (001) cleaving plane.

Finally, the momentum distribution of ARPES intensity at 400 meV binding energy, just below the calculated Fermi level of $Bi_{14}Rh_3I_9$, clearly shows a hexagonal pattern (Fig. 3c), as is

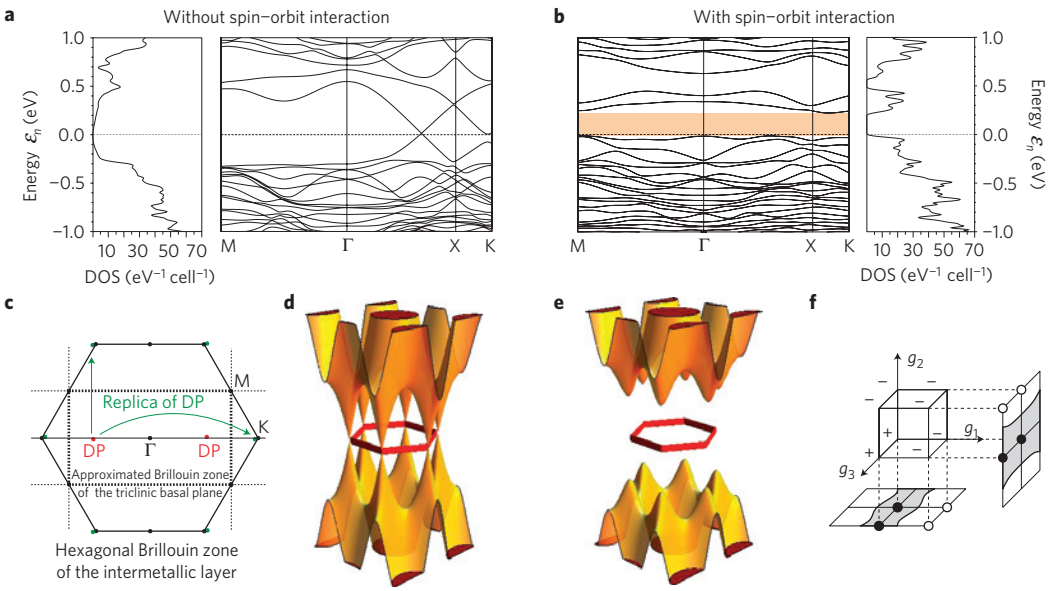

Figure 2 | Electronic structure of $Bi_{14}Rh_3I_9$ with and without spin–orbit interaction. a, Scalar relativistic band structure of triclinic $Bi_{14}Rh_3I_9$. On the line ΓX a Dirac cone is present. **b**, Fully relativistic band structure where the spin–orbit interaction opens up a gap of ~210 meV (shaded area). **c**, Projections of the Dirac points (DP, red) onto the two-dimensional Brillouin zone (dashed lines) of the triclinic basal plane. Replication of the DP (green) to the neighbouring Brillouin zones yields positions close to the K points of the unfolded hexagonal Brillouin zone (solid lines). **d**,**e**, Illustration of the Dirac cones in the situation without spin–orbit interaction (**d**) and the topological gap induced by the spin–orbit interaction (**e**). **f**, Parity eigenvalues at the eight time-reversal-invariant points in the 3D Brillouin zone, where g_3 corresponds to the direction perpendicular to the Bi–Rh planes. The parity eigenvalues lead to the topological invariants $\nu_0;(\nu_1,\nu_2,\nu_3)=0;(0,0,1)$. Projected parities on the planes perpendicular to g_1 and g_2 illustrate the presence of topological edge states on these surfaces.

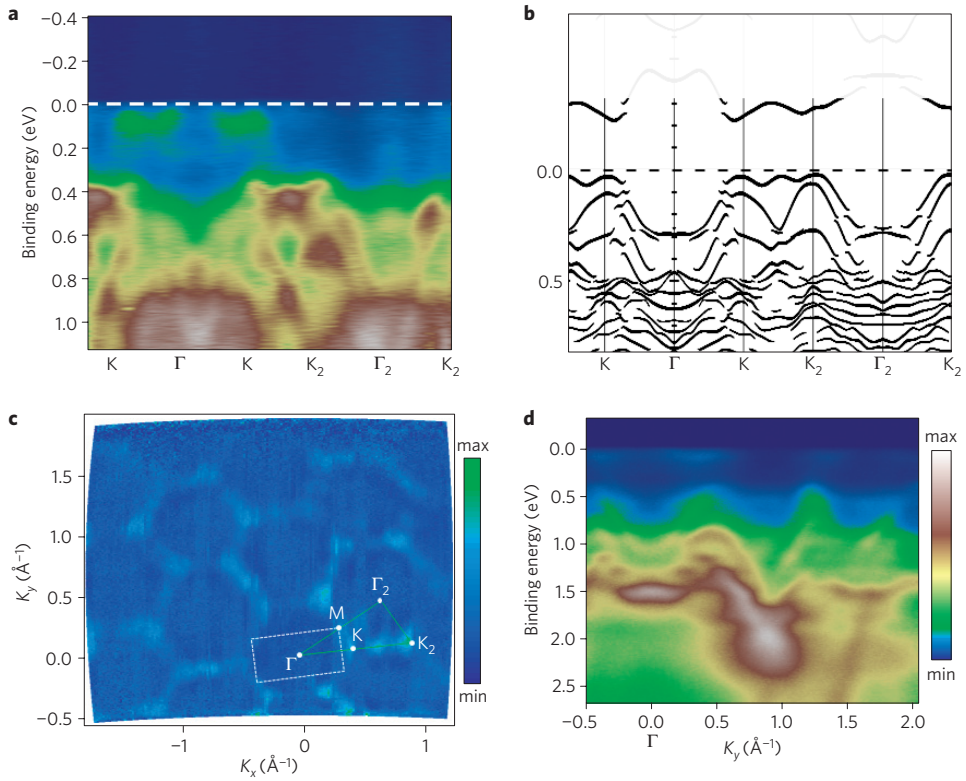

Figure 3 | Band structure as measured by angle-resolved photoemission[26] compared to the calculated one. A small amount of electron doping brings the Fermi-level into the conduction band, so that the topological bandgap becomes clearly visible. **a**, Momentum–energy intensity plot along the high-symmetry ΓK direction of the unfolded Brillouin zone. **b**, Unfolded fully relativistic band structure along the same direction. **c**, Momentum distribution at 0.4 eV binding energy integrated within a 50 meV window. White dashed lines show the trigonal, surface projected Brillouin zone. **d**, Typical momentum–energy distribution taken along the cut that corresponds to $k_x = 0$ in **c**.

expected from the band-structure calculations where the top of the valence band is formed by a dispersive feature that is relatively flat between the K points. The hexagonal pattern justifies the unfolding of the Brillouin zone carried out to facilitate the comparison to ARPES. At the same time its slight irregularity reflects the overall triclinic crystal symmetry.

The hexagons observed in ARPES emphasize the structural and electronic similarities of $Bi_{14}Rh_3I_9$ to graphene, which again it shares with the chemically and structurally closely related compound $Bi_{13}Pt_3I_7$ (refs 24,25), for instance. The compelling difference with graphene is that the large SOC drives $Bi_{14}Rh_3I_9$ electronically into a topologically insulating state, corresponding to a 3D stack of 2D quantum spin Hall states, which is very different from the strong topological insulator states observed so far in bulk materials such as Bi_2Se_3 or Bi_2Te_3 and which is predicted to leave marked signatures on electronic transport through its spin-polarized, stacked quasi-1D topological surface states[22,23].

Received 14 November 2012; accepted 15 January 2013; published online 10 March 2013

References

1. Kane, C. L. & Mele, E. J. Z_2 topological order and the quantum spin Hall effect. *Phys. Rev. Lett.* **95,** 146802 (2005).
2. Kane, C. L. & Mele, E. J. Quantum spin Hall effect in graphene. *Phys. Rev. Lett.* **95,** 226801 (2005).
3. Zhang, H. *et al.* Topological insulators in Bi_2Se_3, Bi_2Te_3 and Sb_2Te_3 with a single Dirac cone on the surface. *Nature Phys.* **5,** 438–442 (2009).
4. Bernevig, B. A., Hughes, T. L. & Zhang, S-C. Quantum spin Hall effect and topological phase transition in HgTe quantum wells. *Science* **314,** 1757–1761 (2006).
5. Fu, L., Kane, C. L. & Mele, E. J. Topological insulators in three dimensions. *Phys. Rev. Lett.* **98,** 106803 (2007).
6. Wu, C., Bernevig, B. A. & Zhang, S-C. Helical liquid and the edge of quantum spin hall systems. *Phys. Rev. Lett.* **96,** 106401 (2006).
7. Fu, L. & Kane, C. L. Superconducting proximity effect and Majorana fermions at the surface of a topological insulator. *Phys. Rev. Lett.* **100,** 096407 (2008).
8. Akhmerov, A. R., Nilsson, J. & Beenakker, C. W. J. Electrically detected interferometry of Majorana fermions in a topological insulator. *Phys. Rev. Lett.* **102,** 216404 (2009).
9. Law, K. T., Lee, P. A. & Ng, T. K. Majorana fermion induced resonant Andreev reflection. *Phys. Rev. Lett.* **103,** 237001 (2009).
10. Xia, Y. *et al.* Observation of a large-gap topological-insulator class with a single Dirac cone on the surface. *Nature Phys.* **5,** 398–402 (2009).
11. Chen, Y. L. *et al.* Experimental realization of a three-dimensional topological insulator, Bi_2Te_3. *Science* **325,** 178–181 (2009).
12. Hsieh, D. *et al.* Observation of time-reversal-protected single-Dirac-cone topological-insulator states in Bi_2Te_3 and Sb_2Te_3. *Phys. Rev. Lett.* **103,** 146401 (2009).
13. Kuroda, K. *et al.* Experimental verification of $PbBi_2Te_4$ as a 3D topological insulator. *Phys. Rev. Lett.* **108,** 206803 (2012).
14. König, M. *et al.* Quantum spin Hall insulator state in HgTe quantum wells. *Science* **318,** 766–770 (2007).
15. Brüne, C. *et al.* Quantum Hall effect from the topological surface states of strained bulk HgTe. *Phys. Rev. Lett.* **106,** 126803 (2011).
16. Min, H. *et al.* Intrinsic and Rashba spin–orbit interactions in graphene sheets. *Phys. Rev. B* **74,** 165310 (2006).
17. Fu, L. & Kane, C. L. Topological insulators with inversion symmetry. *Phys. Rev. B* **76,** 045302 (2007).
18. Moore, J. E. & Balents, L. Topological invariants of time-reversal-invariant band structures. *Phys. Rev. B* **75,** 121306 (2007).
19. Roy, R. Topological phases and the quantum spin Hall effect in three dimensions. *Phys. Rev. B* **79,** 195322 (2009).
20. Koepernik, K. & Eschrig, H. Full-potential nonorthogonal local-orbital minimum-basis band-structure scheme. *Phys. Rev. B* **59,** 1743–1757 (1999).
21. Altland, A. & Zirnbauer, M. R. Nonstandard symmetry classes in mesoscopic normal-superconducting hybrid structures. *Phys. Rev. B* **55,** 1142–1161 (1997).
22. Mong, R. S. K., Bardarson, J. H. & Moore, J. E. Quantum transport and two-parameter scaling at the surface of a weak topological insulator. *Phys. Rev. Lett.* **108,** 076804 (2012).
23. Ringel, Z., Kraus, Y. & Stern, A. The strong side of weak topological insulators. *Phys. Rev. B* **86,** 045102 (2012).
24. Ruck, M. $Bi_{13}Pt_3I_7$: Ein Subiodid mit einer pseudosymmetrischen Schichtstruktur. *Z. Anorg. Allg. Chem.* **623,** 1535 (1997).
25. Ruck, M. From the metal to the molecule—ternary bismuth subhalides. *Angew. Chem. Int. Ed.* **40,** 1182–1193 (2001).
26. Borisenko, S. V. One-cubed ARPES user facility at BESSY II. *Synchrotron Radiat. News* **25,** 6–11 (2012).

Acknowledgements

We acknowledge the help of S. Thirupathaiah, T. Kim and J. Maletz at the ARPES beamline and the grants: BO 1912/3-1, BO 1912/2-2 and ZA 654/1-1. We thank M. Kaiser and A. Gerisch for contributions in solving the crystal structure. We are indebted to ZIH TU Dresden for the provided computational facilities.

Author contributions

B.R. and M. Ruck. planned and carried out the material synthesis and X-ray analysis. S.B., V.Z. and B.B. planned and carried out the ARPES experiments. S.B. prepared the samples and analysed the ARPES data. J.v.d.B., C.O. and M. Richter developed the theory with A.I., B.R., K.K. and M. Richter performing the band-structure calculations and K.K. implementing the calculation of topological invariants into the FPLO code. A.I. analysed the chemical bonding. J.v.d.B. and M. Ruck wrote the paper with contributions from all co-authors. M. Ruck, B.B. and J.v.d.B. supervised the project.

Additional information

Supplementary information is available in the online version of the paper. Reprints and permissions information is available online at www.nature.com/reprints. Correspondence and requests for materials should be addressed to J.v.d.B.

Competing financial interests

The authors declare no competing financial interests.